Li–O_2 Batteries

International Edition: DOI: 10.1002/anie.201410786
German Edition: DOI: 10.1002/ange.201410786

Three Dimensionally Ordered Mesoporous Carbon as a Stable, High-Performance Li–O_2 Battery Cathode**

Jin Xie, Xiahui Yao, Qingmei Cheng, Ian P. Madden, Paul Dornath, Chun-Chih Chang, Wei Fan, and Dunwei Wang**

Abstract: *Enabled by the reversible conversion between Li_2O_2 and O_2, Li–O_2 batteries promise theoretical gravimetric capacities significantly greater than Li-ion batteries. The poor cycling performance, however, has greatly hindered the development of this technology. At the heart of the problem is the reactivity exhibited by the carbon cathode support under cell operation conditions. One strategy is to conceal the carbon surface from reactive intermediates. Herein, we show that long cyclability can be achieved on three dimensionally ordered mesoporous (3DOm) carbon by growing a thin layer of FeO_x using atomic layer deposition (ALD). 3DOm carbon distinguishes itself from other carbon materials with well-defined pore structures, providing a unique material to gain insight into processes key to the operations of Li–O_2 batteries. When decorated with Pd nanoparticle catalysts, the new cathode exhibits a capacity greater than 6000 mAh g_{carbon}^{-1} and cyclability of more than 68 cycles.*

Metal–air batteries have been studied for decades, with significant interest focusing on Li–O_2 batteries as a result of their potentially high gravimetric capacities.[1–4] The key to the successful operation of a Li–O_2 battery is the control over Li_2O_2 formation and decomposition. Many of the observed failing mechanisms are connected to these two processes.[5,6] For instance, discharge products other than Li_2O_2 are often found difficult to decompose upon recharge, leading to fast capacity fading. Side reactions other than Li_2O_2 formation and decomposition degrade the electrode or the electrolyte or both.[7,8] Synergistic effects between the carbon support and the electrolyte have been recently recognized to contribute to these side reactions.[9] Existing reports detailing the formation of Li_2O_2 deposits concerning, for example, their sizes, morphologies, and crystallinity, vary, rendering it difficult to gain a global understanding of the key processes involved in Li–O_2 battery operation.[10–13] The issue is compounded in part by the poorly defined pore structures and surfaces of reported carbon supports. With this in mind, it is clear that detailed studies of Li_2O_2 formation and decomposition on a cathode support of well-defined structures and surfaces should be of great value.[14–17] In this context, three dimensionally ordered mesoporous (3DOm) carbon, an inverse replica of face-centered-cubic (FCC) close-packed structures (Figure 1 A), presents a unique opportunity to understand the operation of Li–O_2 batteries.[18,19]

The size of the pores and the windows connecting the pores in the 3DOm carbon can be independently tuned, as has been reported previously.[18] This feature makes 3DOm carbon distinctly different from other carbon supports (e.g., super P or Vulcan carbon) where well-defined pores in the range of tens of nanometers are not available.[20,21] In this regard, 3DOm carbon also distinguishes itself from carbon nanotubes whose sidewalls are essentially open spaces.[22] Similarly, spaces between randomly arranged graphene sheets (and other graphene derivatives including reduced graphene oxides) are also less than uniform.[23] To demonstrate the potential applicability of the well-defined pores, we next study how the cyclability depends on the pore sizes. Our understanding as depicted in Figure 1 B is based on the following assumptions. First, side reactions other than Li_2O_2 formation and decomposition on the surfaces of carbon are inevitable during Li–O_2 battery operations.[24] Second, these reactions result in accumulation of byproducts that will eventually clog the pores of 3DOm carbon.[5,7,25] Third, once the pores are clogged, the volume accessible for Li_2O_2 deposition drops dramatically, resulting in cell failure. As smaller pores correspond to greater surface-to-volume ratios, they will be clogged more easily than bigger pores. We therefore expect poorer cyclability on 3DOm carbon of smaller pores. This expectation was indeed verified, as shown in Figure 1 C. Even by limiting the discharge capacity (C) to a modest 500 mAh g_{carbon}^{-1}, less than 10% of the total achievable capacity, we observed severe capacity fading by the 15th cycle of recharge for 3DOm carbon with 35 nm pores. A poorer cycling performance was witnessed on 3DOm carbon of smaller pores (with capacity fading by the 6th to the 7th cycle for 12 nm pores; see Figure 1 C and Figure S5 in the Supporting Information).

[*] J. Xie,[+] X. Yao,[+] Q. Cheng,[+] I. P. Madden, Prof. Dr. D. Wang
Department of Chemistry, Merkert Chemistry Center
Boston College, 2609 Beacon St., Chestnut Hill, MA 02467 (USA)
E-mail: dunwei.wang@bc.edu

P. Dornath, C.-C. Chang, Prof. Dr. W. Fan
Department of Chemical Engineering, University of Massachusetts
686 North Pleasant St., Amherst, MA 01003, (USA)
E-mail: wfan@engin.umass.edu

[+] These authors contributed equally to this work.

[**] The work is supported by Boston College, in part by the National Science Foundation (DMR 1317280). The work on the synthesis of 3DOm carbon and textual analysis is partially supported by the Catalysis Center for Energy Innovation, an Energy Frontier Research Center funded by the U.S. Department of Energy, Office of Science, and Office of Basic Energy Sciences under Award No. DE-SC0001004. D.W. is an Alfred P. Sloan Fellow. We thank G. McMahon, G. Chen, and L. Chou for their technical assistance and Z. Qin for insightful discussion.

Supporting information for this article is available on the WWW under http://dx.doi.org/10.1002/anie.201410786.

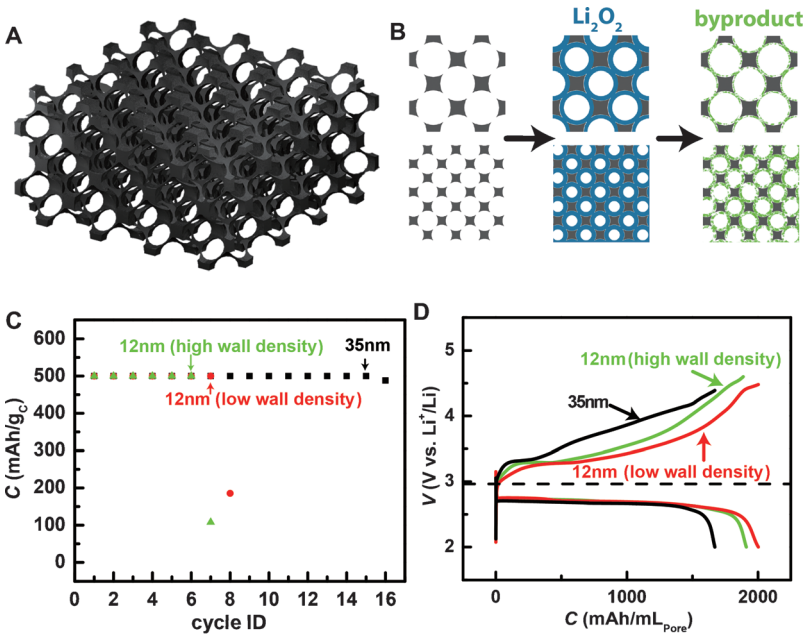

Figure 1. Structure and cycling performance of 3DOm carbon with well-defined pore sizes. A) 3D model for the structure of 3DOm carbon showing only the large pores. B) Simplified 2D representation of the formation and accumulation of byproducts on 3DOm carbon with large (top) and small pores (bottom). Images show pristine carbon (left), carbon with the Li_2O_2 discharge product (middle), and the product after recharge (right), where green deposits represent byproducts that cannot be easily decomposed. C) Cycling performance of bare 3DOm carbon of different pore sizes: 3DOm carbon with 35 nm pores (black) and 12 nm pores with high (green) and low (red) wall densities. High wall density refers to carbon with fewer mesopores, low wall density refers to that with more mesopores (Figure S1). Capacity is limited to 500 mAh g_{carbon}^{-1}, rate = 100 mA g_{carbon}^{-1}. D) Discharge/charge curves normalized to pore volumes. The discharge potential was constrained to $\geq$ 2 V (vs. Li^+/Li).

It is anticipated that capacity depends only on the accessible mesopores (i.e., pores defined by the silica beads) but not the micropores in the carbon walls ($d \leq 2$ nm, where d is the pore diameter) because the micropores are too small to support Li_2O_2 deposition. Indeed, upon deep discharge, the capacities, normalized to the volumes specific to the large pores, are comparable, as shown in Figure 1 D (35 nm pores: $C = 1700$ mAh mL_{pore}^{-1}, 12 nm pores: $C = 2000$ mAh mL_{pore}^{-1}; see Figures S1 and S2 and Table S1). Most strikingly, negligible difference is evident between the capacities measured on 3DOm carbon of similar pore sizes (circa 12 nm) but with different micropore volumes (see the green and red traces in Figure 1 D), strongly supporting that micropores do not contribute to the capacities.

Next, we seek to address an important concern in using carbon supports for Li–O_2 battery operations, specifically the reactivity of carbon.[26] Increasing evidence suggests that carbon is unstable against O_2^- during discharge.[24] Carbon is also reactive under high recharge potentials.[9,25] Our strategy to address the issue is to physically separate the carbon surface from Li_2O_2, any reaction intermediates, as well as the electrolyte. The goal is achieved by growing a thin, uniform layer of metal oxides on 3DOm carbon (Figure 2 A). As a result of the synthetic procedure employed to prepare 3DOm carbon, its surface is inherently hydrophilic, ideal for growing oxides by atomic layer deposition (ALD). The benefit of ALD growth is that it affords complete coverage of the surface with minimum defects. In this study, we demonstrate that amorphous FeO_x is an effective protection layer for 3DOm carbon. The uniformity of the FeO_x growth is confirmed by the following experiments. First, pore size distributions as shown in Figure 2 B clearly verify that the average pore sizes have been decreased from 33.0 nm to 30.2 nm, corresponding to a wall thickness of 1.4 nm for FeO_x, consistent with what is expected from a 50-cycle ALD growth. Second, the bright-field transmission electron micrographs (TEM) before and after the ALD treatment (Figure 2 C) unambiguously confirm the deposition of FeO_x. Finally, the existence and distribution of FeO_x can be visualized by Raman mapping (see Figure S3 in the Supporting Information). In combination, the surface textural analyses, TEM micrographs, and Raman mapping confirm that the coverage of FeO_x on the surface of the 3DOm carbon is uniform. The uniform FeO_x coating is expected to provide the desired protection that should minimize side reactions inherent to bare carbon surfaces.

The separation of the carbon surface from the reaction intermediates also hinders the well-known activity of carbon in oxygen reduction reactions (ORR). At first glance this may seem counterintuitive, as after all the first step of Li–O_2 battery discharge is to reduce oxygen. As such, the ORR activity of carbon would be a beneficial property. However, as shown in Figure 3 A (upper panel), the ORR activity of carbon promotes Li_2O_2 formation randomly on the surface of

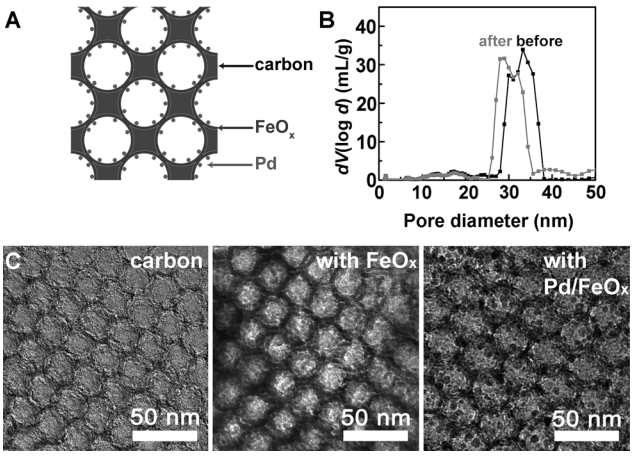

Figure 2. Protection of 3DOm carbon by FeO_x and subsequent functionalization with Pd nanoparticle catalysts. A) Overview of the design strategy. B) Pore size distributions confirm a uniform decrease in the pore diameter from 33.0 nm to 30.2 nm. C) TEM images showing pristine 3DOm carbon (left) and the surface after FeO_x deposition (middle) and subsequent decoration with Pd nanoparticles (right).

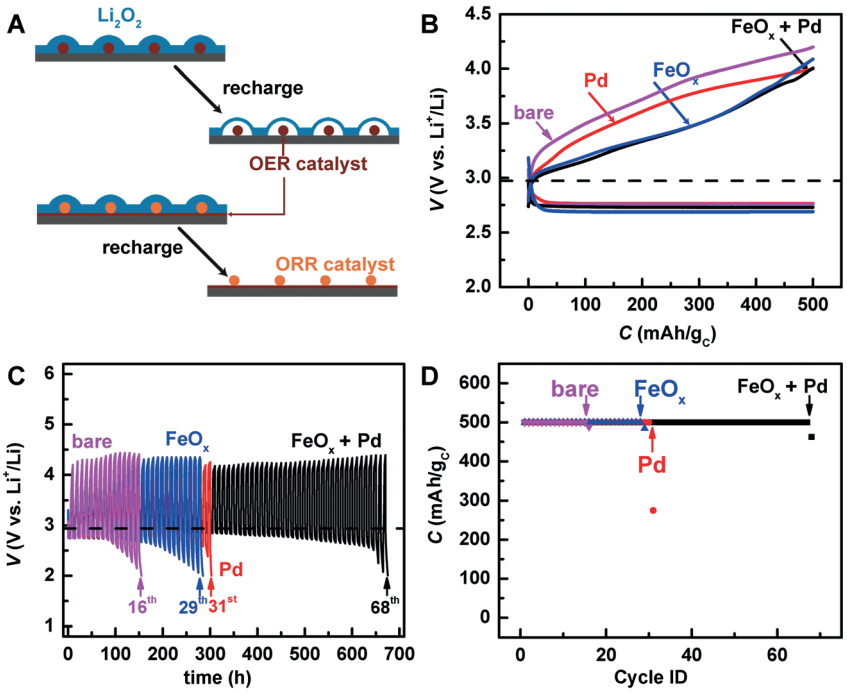

Figure 3. The effect of FeO_x and Pd decoration on the properties of 3DOm carbon. A) The influence of Li_2O_2 deposition on the ORR activity of carbon and the subsequent effects of the FeO_x coating and Pd nanoparticle decoration of the surface. When the FeO_x coating (an OER catalyst) is combined with Pd (an ORR catalyst), the decomposition of Li_2O_2 can be more complete. B) The first cycle voltage–capacity discharge/recharge curves for the materials (current density = 100 mA g_C^{-1}). C) Charge/discharge curves and D) cycling data for each of the cells. More complete decomposition of Li_2O_2 corresponds to better cyclability in the deep discharge/recharge cycles.

carbon, at or away from sites of oxygen evolution reactions (OER). Note that OER catalysts are necessary to decompose Li_2O_2 at relatively low recharge overpotentials.[27] Li_2O_2 which is deposited far away from OER sites is difficult to decompose, increasing the need for overpotentials and driving up the recharge potentials. Even worse, they may remain during the following cycles, accumulate, and eventually lead to capacity fading. The FeO_x coating is a known OER catalyst in aqueous systems.[28] We therefore set out to examine whether the FeO_x coating may catalyze the decomposition of Li_2O_2 in non-aqueous electrolytes. As shown in Figure 3B (see also the following discussion), the OER activity of FeO_x in dimethoxyethane (DME) is indeed evident. As such, their uniform presence on the carbon surface ensures complete decomposition of Li_2O_2 at relatively low overpotentials (Figure 3A, lower panel). To compensate for the loss of ORR activity, Pd nanoparticles, one of the best-known ORR catalysts in both aqueous and non-aqueous electrolytes (Figure 2A),[14,29] were grown on the 3DOm carbon surface by ALD after the deposition of FeO_x. The successful growth of uniform Pd nanoparticles within 3DOm carbon pores is confirmed by TEM in Figure 2C (far right panel).

The efficacy of the above-outlined material design and preparation strategy is clear. Figure 3B shows that the average discharge potential measured on bare 3DOm carbon was 2.76 V (versus Li^+/Li), representing an overpotential of 0.20 V. The overpotential increased to 0.26 V when carbon was covered by FeO_x, but dropped back to 0.23 V with Pd nanoparticle deposition. Similarly, bare 3DOm carbon exhibited high recharge overpotentials (0.82 V). Adding Pd led to a decrease to 0.68 V because Pd is also a moderately effective OER catalyst. The presence of FeO_x gave rise to the largest overpotential decrease, in the presence or the absence of Pd nanoparticles (0.48 V and 0.51 V, respectively). The result strongly supports that OER were primarily catalyzed by FeO_x but not Pd, a desired feature of our design principle for this material (Figure 3A).

The most important goal we hope to achieve by deposition of FeO_x and Pd on the 3DOm carbon surface is to increase the cyclability of Li–O_2 batteries, because better controls over Li_2O_2 formation and decomposition are expected to correspond to better cyclability. To evaluate the cathode performance and in accordance with the most common established practices, we limited the capacity to 500 mAh g^{-1} and recorded the charge/discharge behaviors of the cells (Figure 3C). When the discharge potential dropped below 2.0 V, we considered the cell to have failed. Figures 3C and 3D show that a bare 35 nm 3DOm carbon cathode failed after the 16th cycle. Addition of Pd improved the cyclability with the cell failing after the 31st cycle, presumably as a result of the OER properties of Pd. The presence of FeO_x significantly stabilized the cathode, and the cell did not fail until the 68th cycle. This value represents the highest cycling number, to our knowledge, obtained on a carbon-based cathode support in a DME-based electrolyte. As the decomposition of all established electrolyte systems is a recognized issue, we expect that the cell performance will eventually degrade. Within this context, we were pleased that the lifetime of a carbon cathode could be extended fourfold by a simple FeO_x coating and decoration with Pd nanoparticles.

We next set out to confirm that the measured performance is indeed as a result of the formation and decomposition of Li_2O_2. First, the X-ray diffraction pattern (Figure 4A) unambiguously confirmed the formation of Li_2O_2 upon discharge. The peaks at 32.9, 35.0, and 40.7° agreed well with documented diffraction peaks of Li_2O_2 (JCPDS 74-0115). Notably, no peaks corresponding to Li_2CO_3, an important undesired byproduct of Li–O_2 battery operation, were found in the XRD pattern. Upon recharge, the Li_2O_2 diffraction peaks disappeared. Significantly, at the 61st cycles, the diffraction peaks of Li_2O_2 were still prominent whereas no Li_2CO_3 peaks were detected. Next, X-ray photoelectron spectroscopy (XPS) was used to confirm the existence of Li_2O_2 from O 1s spectra. Before discharge, only species corresponding to iron oxide were identified: the peak located at 529.9 eV is

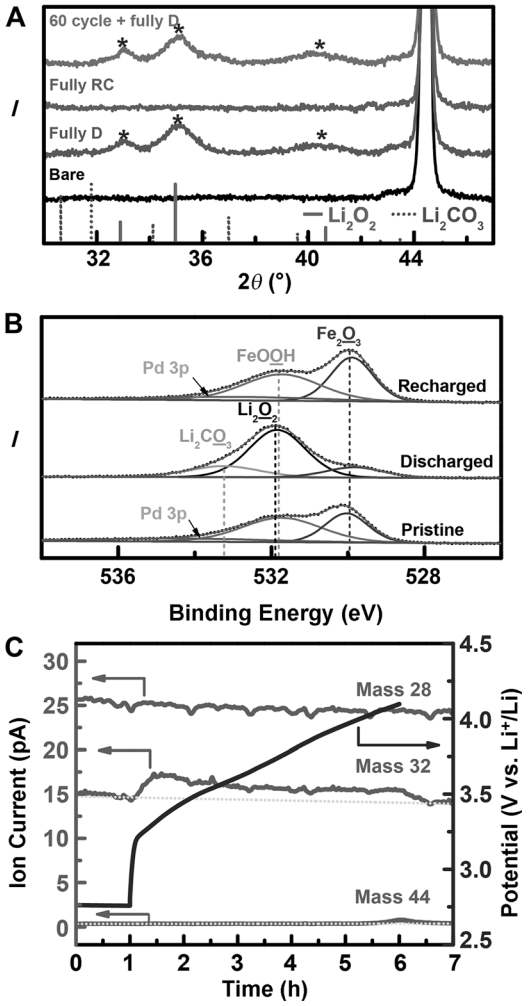

Figure 4. A) X-ray diffraction peaks before discharge (bare), after the 1st cycle discharge (fully D), the 1st cycle recharge (fully RC), and fully discharged after 60 cycles of operations (60 cycle + fully D). B) X-ray photoelectron spectra before discharge (bottom), after discharge (middle), and after recharge (top). Deconvoluted peaks are labelled with the element of interest underlined. C) Differential electrochemical mass spectrometry (DEMS) experiment to quantify the gaseous recharge product. N_2 (mass 28) is used as a control and the evolution of O_2 (mass 32), and CO_2 (mass 44) are detected. The corresponding voltages were plotted against the right axis.

attributed to O^{2-} in the lattice of Fe_2O_3 and the peak at 531.7 eV to surface hydroxide terminal groups on Fe_2O_3. A third, much less prominent broad peak at 534.2 eV was assigned to Pd $3p_{3/2}$ of oxides on Pd nanoparticle surfaces. After discharge, three distinct peaks were obtained. Among them, the peak at 529.9 eV (from iron oxide) remained unchanged. At 531.9 eV was a new, most significant peak corresponding to Li_2O_2. The peak at 533.4 eV increased in intensity. It can be assigned to O in Li_2CO_3 as a result of the short exposure of sample to the ambient air before loading into the XPS instrument. Upon recharge, the spectrum was nearly identical to that measured before discharge.

Third, differential electrochemical mass spectrometry (DEMS) was used to quantify the gaseous recharge product. For this set of experiments, tetraethylene glycol dimethyl ether (TEGDME) was chosen as the electrolyte solvent because of its relatively low vapor pressures. During the 1st cycle recharge, O_2 accounted for 96.6% of the total gas evolved. Despite the protection of the carbon with FeO_x, the loss of CO_2 was detected (3.4% of the total amount). It is noteworthy that the O_2 diffusion coefficient in TEGDME ($2.17\times10^{-6}\,cm^2\,s^{-1}$) is lower than in DME ($1.22\times10^{-5}\,cm^2\,s^{-1}$),[30] which was the primary solvent used for all characterization experiments other than DEMS. Consequently, the average recharge potentials in TEGDME (3.69 V) was greater than in DME (3.44 V). We therefore expect more severe side reactions when TEGDME is used. The formation and decomposition of Li_2O_2 on a protected 3DOm carbon electrode was also visualized by scanning electron microscopy (SEM; Figure S10). It is noteworthy that the reported morphologies and sizes of Li_2O_2 deposits vary depending on the cathode materials employed and the detailed discharge conditions. For instance, recent studies reported the formation of Li_2O_2 toroids in water-contaminated ether electrolytes and other electrolytes with high donor numbers.[31,32] In the present study, toroid formation was not detected on the 3DOm carbon electrode (see the Supporting Information for test conditions and Figure S13 for the cell design).

Before the full potential of Li–O_2 batteries can be realized, significant advances in many areas, including the discovery of stable electrolytes and anodes, are necessary. Among them, control over the product (Li_2O_2 in the case of the Li–O_2 battery) formation and decomposition are critical. The availability of suitable materials that can facilitate detailed studies of the processes will contribute significantly to this field. Within this context, 3DOm carbon offers unprecedented opportunities. The demonstrated high capacity and preferential product deposition within the large pores of 3DOm carbon provide a solid foundation for the preparation of high-performance Li–O_2 batteries. A facile FeO_x ALD growth, in conjunction with decoration of the material with ligand-free Pd nanoparticles as an ORR catalyst, readily addresses the inherent reactivity of carbon and extends the cyclability from 16 to 68 cycles. Importantly, the 3DOm carbon platform allows for control over the size and location of Li_2O_2 deposition. We anticipate that 3DOm carbon will play an increasingly more important role in the field of energy storage.

Keywords: atomic layer deposition · electrochemistry · energy storage · mesoporous materials · supported catalysts

How to cite: *Angew. Chem. Int. Ed.* **2015**, *54*, 4299–4303
Angew. Chem. **2015**, *127*, 4373–4377

[1] K. Abraham, Z. Jiang, *J. Electrochem. Soc.* **1996**, *143*, 1–5.
[2] P. Hartmann, C. L. Bender, M. Vračar, A. K. Dürr, A. Garsuch, J. Janek, P. Adelhelm, *Nat. Mater.* **2013**, *12*, 228–232.
[3] X. Ren, Y. Wu, *J. Am. Chem. Soc.* **2013**, *135*, 2923–2926.
[4] Y. Li, H. Dai, *Chem. Soc. Rev.* **2014**, *43*, 5257–5275.
[5] B. D. McCloskey, D. S. Bethune, R. M. Shelby, G. Girishkumar, A. C. Luntz, *J. Phys. Chem. Lett.* **2011**, *2*, 1161–1166.

[6] Y. C. Lu, B. M. Gallant, D. G. Kwabi, J. R. Harding, R. R. Mitchell, M. S. Whittingham, Y. Shao-Horn, *Energy Environ. Sci.* **2013**, *6*, 750 – 768.
[7] B. D. McCloskey, A. Speidel, R. Scheffler, D. C. Miller, V. Viswanathan, J. S. Hummelshøj, J. K. Nørskov, A. C. Luntz, *J. Phys. Chem. Lett.* **2012**, *3*, 997 – 1001.
[8] B. D. McCloskey, D. S. Bethune, R. M. Shelby, T. Mori, R. Scheffler, A. Speidel, M. Sherwood, A. C. Luntz, *J. Phys. Chem. Lett.* **2012**, *3*, 3043 – 3047.
[9] M. M. Ottakam Thotiyl, S. A. Freunberger, Z. Q. Peng, P. G. Bruce, *J. Am. Chem. Soc.* **2013**, *135*, 494 – 500.
[10] B. M. Gallant, D. G. Kwabi, R. R. Mitchell, J. Zhou, C. V. Thompson, Y. Shao-Horn, *Energy Environ. Sci.* **2013**, *6*, 2518 – 2528.
[11] J.-J. Xu, Z.-L. Wang, D. Xu, L.-L. Zhang, X.-B. Zhang, *Nat. Commun.* **2013**, *4*, 2438.
[12] E. Yilmaz, C. Yogi, K. Yamanaka, T. Ohta, H. R. Byon, *Nano Lett.* **2013**, *13*, 4679 – 4684.
[13] B. D. Adams, C. Radtke, R. Black, M. L. Trudeau, K. Zaghib, L. F. Nazar, *Energy Environ. Sci.* **2013**, *6*, 1772 – 1778.
[14] J. Lu, Y. Lei, K. C. Lau, X. Y. Luo, P. Du, J. G. Wen, R. S. Assary, U. Das, D. J. Miller, J. W. Elam, H. M. Albishri, D. Abd El-Hady, Y. K. Sun, L. A. Curtiss, K. Amine, *Nat. Commun.* **2013**, *4*, 2383.
[15] J. Xie, X. Yao, I. P. Madden, D.-E. Jiang, L.-Y. Chou, C.-K. Tsung, D. Wang, *J. Am. Chem. Soc.* **2014**, *136*, 8903 – 8906.
[16] S. J. Kang, T. Mori, S. Narizuka, W. Wilcke, H.-C. Kim, *Nat. Commun.* **2014**, *5*, 3937.
[17] Z. Peng, S. A. Freunberger, Y. Chen, P. G. Bruce, *Science* **2012**, *337*, 563 – 566.
[18] W. Fan, M. A. Snyder, S. Kumar, P.-S. Lee, W. C. Yoo, A. V. McCormick, R. Lee Penn, A. Stein, M. Tsapatsis, *Nat. Mater.* **2008**, *7*, 984 – 991.
[19] K. A. Cychosz, X. Guo, W. Fan, R. Cimino, G. Y. Gor, M. Tsapatsis, A. V. Neimark, M. Thommes, *Langmuir* **2012**, *28*, 12647 – 12654.
[20] Z. Guo, D. Zhou, X. Dong, Z. Qiu, Y. Wang, Y. Xia, *Adv. Mater.* **2013**, *25*, 5668 – 5672.
[21] N. Ding, S. W. Chien, T. S. A. Hor, R. Lum, Y. Zong, Z. Liu, *J. Mater. Chem. A* **2014**, *2*, 12433 – 12441.
[22] Z. Jian, P. Liu, F. Li, P. He, X. Guo, M. Chen, H. Zhou, *Angew. Chem. Int. Ed.* **2014**, *53*, 442 – 446; *Angew. Chem.* **2014**, *126*, 452 – 456.
[23] B. Sun, X. Huang, S. Chen, P. Munroe, G. Wang, *Nano Lett.* **2014**, *14*, 3145 – 3152.
[24] D. M. Itkis, D. A. Semenenko, E. Y. Kataev, A. I. Belova, V. S. Neudachina, A. P. Sirotina, M. Hävecker, D. Teschner, A. Knop-Gericke, P. Dudin, A. Barinov, E. A. Goodilin, Y. Shao-Horn, L. V. Yashina, *Nano Lett.* **2013**, *13*, 4697 – 4701.
[25] B. D. McCloskey, A. Valery, A. C. Luntz, S. R. Gowda, G. M. Wallraff, J. M. Garcia, T. Mori, L. E. Krupp, *J. Phys. Chem. Lett.* **2013**, *4*, 2989 – 2993.
[26] M. M. Ottakam Thotiyl, S. A. Freunberger, Z. Peng, Y. Chen, Z. Liu, P. G. Bruce, *Nat. Mater.* **2013**, *12*, 1050 – 1056.
[27] R. Black, J.-H. Lee, B. Adams, C. A. Mims, L. F. Nazar, *Angew. Chem. Int. Ed.* **2013**, *52*, 392 – 396; *Angew. Chem.* **2013**, *125*, 410 – 414.
[28] Y. Lin, S. Zhou, S. W. Sheehan, D. Wang, *J. Am. Chem. Soc.* **2011**, *133*, 2398 – 2401.
[29] Y.-C. Lu, H. A. Gasteiger, Y. Shao-Horn, *J. Am. Chem. Soc.* **2011**, *133*, 19048 – 19051.
[30] C. O. Laoire, S. Mukerjee, K. M. Abraham, E. J. Plichta, M. A. Hendrickson, *J. Phys. Chem. C* **2010**, *114*, 9178 – 9186.
[31] L. Johnson, C. Li, Z. Liu, Y. Chen, S. A. Freunberger, P. C. Ashok, B. B. Praveen, K. Dholakia, J.-M. Tarascon, P. G. Bruce, *Nat. Chem.* **2014**, *6*, 1091 – 1099.
[32] N. B. Aetukuri, B. D. McCloskey, J. M. García, L. E. Krupp, V. Viswanathan, A. C. Luntz, *Nat. Chem.* **2015**, *7*, 50 – 56.

Received: November 5, 2014
Revised: January 18, 2015
Published online: February 10, 2015

